Int J Adv Manuf Technol (2015) 79:1607–1621
DOI 10.1007/s00170-015-6936-2

ORIGINAL ARTICLE

Comparative study of the slurry erosion behavior of laser cladded Ni-WC coating modified by nanocrystalline WC and La_2O_3

Parisa Farahmand · Thomas Frosell · Molly McGregor · Radovan Kovacevic

Received: 2 September 2014 / Accepted: 20 February 2015 / Published online: 7 March 2015

Abstract The erosion performance of laser cladded Ni-60 %WC coatings subjected to a controllable abrasive water jet (AWJ) was investigated. The erosion resistance of Ni-60 %WC coatings at varied linear laser energy (from 315 to 700 J/mm) was examined under different impinging angles of a slurry jet. The chemical composition of coatings was modified by nanocrystalline WC powder and the rare earth element (La_2O_3). The erosion value of Ni-60 %WC was reduced to 40 % by decreasing the laser energy from 700 to 315 J/mm. Synthesized coatings with optimal weight fraction of nano-WC particles (5 %) and La_2O_3 (1 %) decreased the average microstructural grain size of the Ni-binder, increased the homogeneity and hardness of the coating, and consequently increased the erosion resistivity. The tribological evaluation of the erosion scars showed a log-linear relationship between coating hardness and volume loss under erosion. Adding nano-WC (5 %) and La_2O_3 (1 %) enhanced the bonding strength between Ni and WC and no pulled out WC particles was observed after erosion test.

Keywords Ni-WC composite coating · Slurry erosion · Nanocrystalline WC · Rare earth element

1 Introduction

Slurry erosion generally describes the metal surface degradation by micro-mechanical deformation/fracture resulting from random impacts of the high velocity liquid with a solid particle suspension. Wear and erosion under slurry erosion conditions such as unprocessed oil, gas, and water mixture are the primary reasons for component damage in the oil and gas industry [1]. During erosion, abrasive particles impose high-strain-rate deformation on the material. The strain rate is in the order of 10^3 to 10^6/s [2]. Continuous impact of slurry particles induces stress in the metal surface, and by exceeding the yield stress, the plastic deformation occurs in or close to the impact region. Additionally, the yield stress of the material coating increases due to strain hardening, and eventually the yield stress becomes equal to the fracture stress. Once this occurs, no further plastic deformation can follow. The material becomes brittle and tends to fragment from subsequent impacts [3].

The components exposed to the slurry-erosion condition require a coating with outstanding material properties. From a surface engineering perspective, hard-facing overlays such as metal matric composites (MMC) offer some unique coating characteristics to protect equipment subjected to erosion. The main beneficial property of the MMC coatings is the combination of a ductile matrix with brittle hard-phase reinforcement. Under the slurry erosion condition, the material removal of MMC coating mainly occurs by binder surface scratching where the scratch width defines the scale of the damage. In such condition, the carbide particles resist the scratch development and deflect the erodent particles, acting as matrix protector [3]. The level of the MMC coating erosion resistance is determined by the combination of erosion conditions and material properties. Microstructural integrity, microhardness, coating composition, carbide grain size, and bonding strength between constituents are the main coating characteristics in the assessment of erosion resistivity [4, 5]. It was shown that there is a log-linear relationship between hardness and volume loss under slurry erosion condition [6]. The erosion rate is also dependent on the major testing factors including test conditions, impact velocity, impinging particle size and shape, erodent type, and impact angle [5].

P. Farahmand · R. Kovacevic (✉)
Center for Laser-aided Manufacturing, Lyle School of Engineering, Southern Methodist University, 3101 Dyer Street, Dallas, TX 75205, USA
e-mail: kovacevi@lyle.smu.edu

T. Frosell · M. McGregor
Halliburton, 2601 E. Belt Line Road, Carrollton, TX 75006, USA

The mechanical properties of the MMC coating strongly depend on microstructure of the binder and the grain size of reinforcing hard phase. The modification of the microstructure and chemical composition in order to enhance the erosion resistance of the coating has gained increasing interest. Using nanoparticles enhance the mechanical properties, crack prevention, and homogeneity of MMC coatings [7]. Cho et al. [8] demonstrated that the size of the carbide particles has a considerable effect on the mechanical properties of the MMC coating. These researchers observed that the composite Young s modulus and tensile strength could be improved by adding the nano-sized particles. E. Yarrapareddy and R. Kovacevic [9] studied the effect of adding 5 % nano-WC on the erosion resistivity of the Ni-60 %WC composite coating. Another approach to enhance the mechanical properties of MMC coatings was based on the addition of the rare earth (RE) elements. RE powders can be decomposed and activated within the molten pool and affect the solidification pattern and surface tension gradients. The effects of cerium oxide (CeO2) and lanthanum oxide (La_2O_3) on the microstructural evolution and enhancement of the tribological properties of nickel-based alloy coatings were investigated by K.L. Wang et al. [10]. Modification of Ni-60 %WC coating by nano-WC and La_2O_3 (RE) in order to improve quality characteristics of the MMC coating such as crack behavior, composite homogeneity, and WC dissolution was studied by the authors [11]. It was found that adding nano-WC (up to 10 %) and La_2O_3 (up to 2 %) to the Ni-60 %WC enhanced the distribution of carbide particles, decreased the crack susceptibility, and increased the microhardness of the coating.

According to the reviewed literature, there are limited studies on studying the effect of coating process parameters on the erosion resistance of MMC coatings. The modification of the microstructure and mechanical properties by changing the chemical composition of coatings is another area that needs more attention. This work encompasses the assessment of erosion behavior of laser cladded Ni-60 %WC MMC coating in the simulated slurry environments. The effect of process cladding parameters on binder microstructure, coating microhardness, and subsequently erosion performance under different impact angles was investigated. Further, the effect of chemical composition enhancement of Ni-binder by adding the RE element (La_2O_3) up to 2 % and reinforcing it with nano-WC particles up to 10 % on the erosion resistance of the coating was studied.

2 Laser cladding assisted with an induction heater

The composite coatings were cladded by laser cladding assisted with an induction heater based on a high-power direct diode laser. A very high heating and cooling rates in cladding process [12, 13] and immense diversity of thermo mechanical properties between binder and carbides [14] increase the residual stress and crack initiation force. Therefore, assisting the laser cladding with an additional heat source for fabricating a homogenous MMC coating is necessity [15]. The laser cladding was performed by using a 8-kW direct diode laser (HPDDL) with 980±10 nm of wavelength. The laser spot had a rectangular shape with the dimensions of 12 mm width (slow axis) and 3 mm length (fast axis). The fast axis was parallel to the scanning direction of the cladding. A cladding head consisted of two symmetrical powder feeding nozzles. A 6-axis KUKA robot as a positioning system and an induction heater as a second heat source were used. Argon gas was used as a carrier gas in the powder delivery and a shielding gas. The composite powders were composed of a mixture of 40 wt% of Ni and 60 wt% of WC/W_2C with spheroidal morphology. It should be noted that 60 wt% WC/W_2C was recognized as the threshold percentage of allowable reinforcement particles in the Ni matrix. An attempt to have a higher percentage than this value would result in cracking of the coating even with the assistance of an induction heater. Nano-WC powder and La_2O_3 powder were synthesized by mixing the Ni-WC particle with three different weight fractions of nano-WC (3-5-10 %) and La_2O_3 powder (0.5-1-2 %) with purity of over 99 %, the powders were mixed by powder mixture and some steel bars were added for crushing and preventing the powder aggregation. Table 1 lists the chemical composition and the size of the powders.

The main processing parameters for cladding the Ni-60 %WC composite coating on mild steel A36 as substrate were laser power, powder flow rate, scanning speed, and preheating temperature. In this study, the selection of process parameters was based on obtaining a defect-free (i.e., crack and inter-run pores) and homogenous Ni-WC coatings. In multi-track laser cladding, an overlap of 25 % was selected as an optimum overlap that minimized the grinding operation after cladding. The coated surfaces of 50×50 mm were prepared by grinding to obtain surface roughness in close range (averagely 1 μm) for slurry erosion tests. The cross section of the coatings was characterized by a scanning electron microscope (SEM), energy dispersive spectroscopy (EDS), microhardness tester, and optical profilometer for measuring the roughness of eroded surfaces. The chemical compositions of the phases for the composite coatings were analyzed by X-ray diffraction (XRD) with irradiation parameters: Cu-Kα radiation source, 40 kV, and 10 mA.

During the cladding, the powder flow rate was kept constant and laser energy as well as scanning speed was changed to obtain three different levels of laser energy densities (315, 400, and 700 J/mm). The laser energy density for coatings modified by nano-WC and La_2O_3 was set at the middle range to demonstrate the effect of synthesis more clearly. Figure 1 shows the SEM micrograph images of Ni-WC coating cross sections. All clads demonstrated a uniform distribution of the WC without cracks and pores except the coatings with 10 wt% nano-WC and with 2 wt% La_2O_3.

In the cross section of coating with 10 % nano-WC, there was some porosity (see Fig. 1f) because there is a high

Table 1 Size and chemical compositions of powders

Elements	B (%)	C (%)	Cr (%)	Co (%)	Fe (%)	Ni (%)	O_2 (%)	Si (%)	Ti (%)	WC (%)
WC/W_2C (80–160 μm)	–	3.99	–	0.008	0.16	0.004	–	–	0.001	96
Ni (1–60 μm)	1.56	0.24	7.46	–	2.55	BAL	0.027	3.4	–	–
Nano-WC (<100 nm)	–	0.06	–	–	0.0001	–	–	0.002	–	99

tendency for clustering and agglomeration of higher percentage of nano-WC particles. Therefore, there is a high concentration of carbon in the nano-WC aggregated areas. During the cladding, carbon would react by atmospheric oxygen. This chemical reaction could be described as follow [15]:

$$C + O_2 \rightarrow CO, CO + O_2 \rightarrow CO_2 \quad (1)$$

An excessive amount of carbon could lead to the formation of CO and CO_2. These elements could become entrapped in the molten pool during rapid solidification and lead to the formation of pores in the clad. It is also found that the addition of 2 % La_2O_3 resulted in a nonhomogeneous particulate dispersion as seen by the accumulation of the WC particles at the bottom of clad (see Fig. 1i). It is shown by other study [11, 16] that an addition of La_2O_3 higher than 1.5 % could cause sharp increase in the oxygen content in the molten pool because of its high reactivity with oxygen [17]. The high content of oxygen in the molten pool decreases the flow ability of the molten material and subsequently non-uniform distribution of the WC particles.

3 Slurry erosion test

The accelerated erosion tests were conducted at room temperature using a Flow IFB 4400 3-axis high-pressure abrasive waterjet (AWJ) cutting machine. Utilizing the waterjet for erosion testing could be found in laboratory erosion testing equipment category [18]. In this machine, the motor-driven pump pressurizes the water and delivers it continuously to the cutting head. During this experiment, the abrasive particles were injected into a mixing chamber by a vacuum created by a high-speed waterjet that could reach the speed of 1000 m/s. The water-abrasive mixture passes through a mixing tube or an accelerator and the mean output speed of jet steam drops to about 300 m/s. The Barton's garnet with angular shape particles was used as eroding material. A fixture was designed and manufactured to hold the samples at different impinging angles. The stand-off distance between the nozzle and sample was set at 1127 mm in order to obtain the approach particles velocity to 56 m/s (i.e., the actual speed of slurry jet) as well as to increase the contact area between the abrasive waterjet and

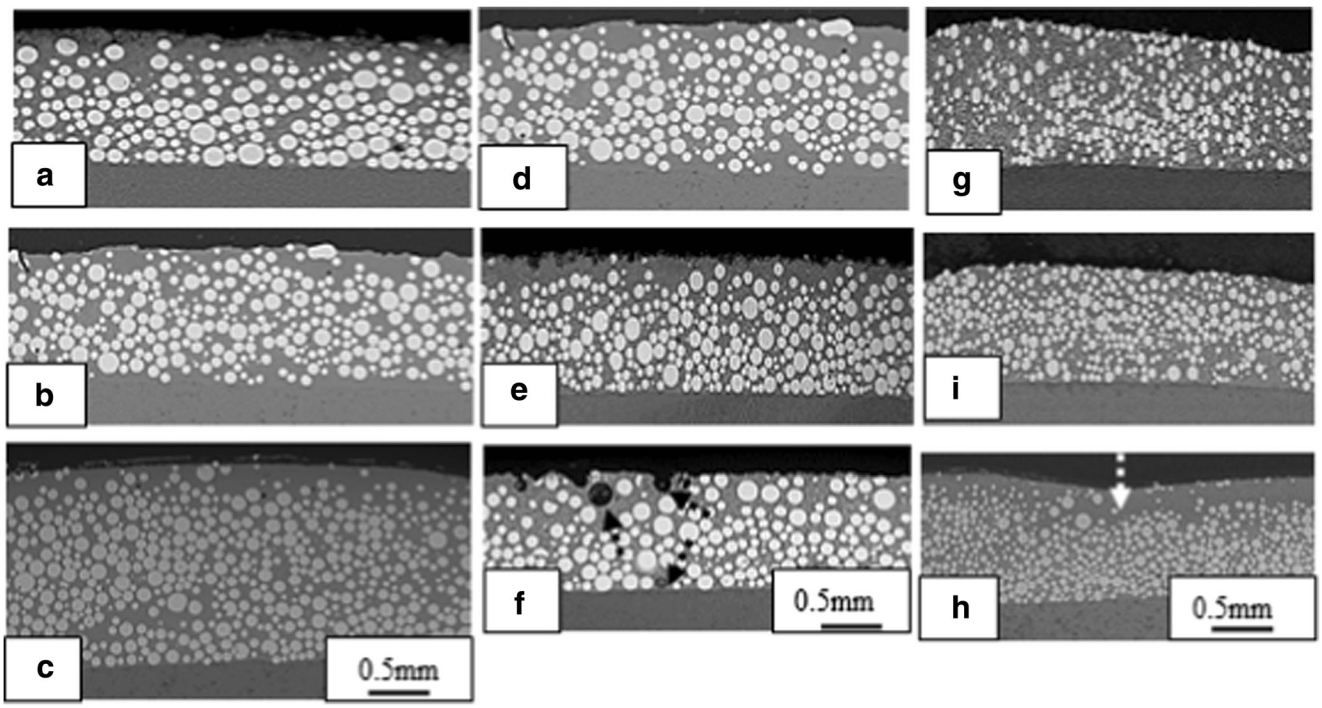

Fig. 1 SEM images of coating cross sections (all images are on the same scale), **a** coating with 315 J/mm linear laser energy, **b** coating with 400 J/mm linear laser energy, **c** coating with 700 J/mm linear laser energy, **d** coating with 3 % nano-WC, **e** coating with 5 % nano-WC, **f** coating with 10 % nano-WC, **g** coating with 0.5 % La_2O_3, **h** coating with 2 % La_2O_3, **i** coating with 1 % La_2O_3

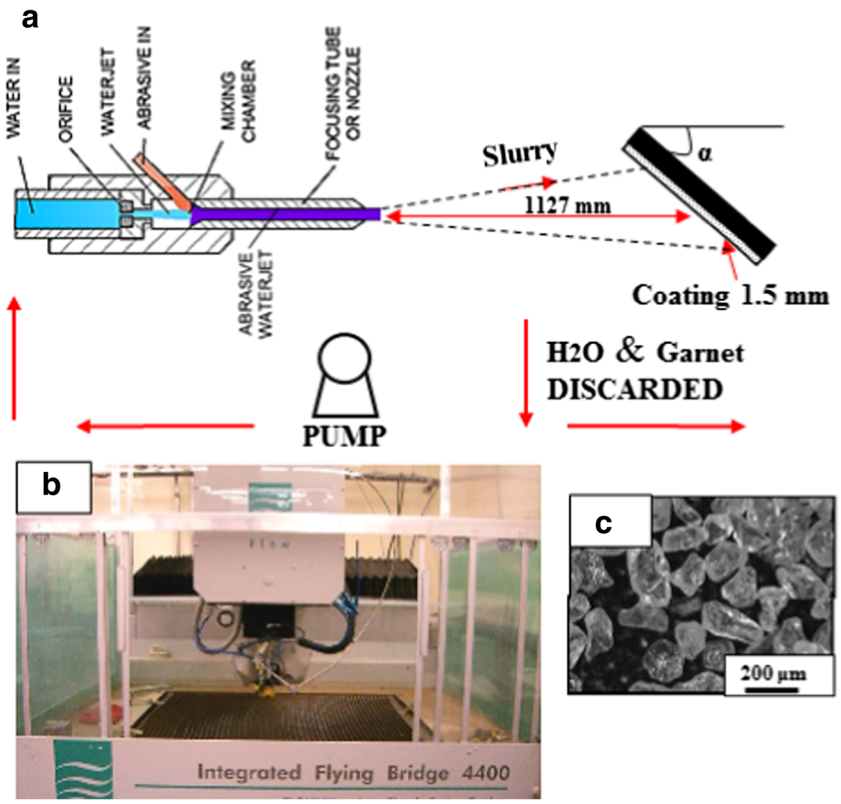

Fig. 2 **a** A schematic view of the slurry erosion test, **b** abrasive water jet machine, **c** abrasive particles

the coated surface (circle with 20 mm in diameter). The schematic view of a slurry erosion test set-up is shown in Fig. 2. Each erosion test lasted for a cumulative time of 210 s and at each 30-s interval time, the test was stopped and the samples were cleaned in an ultrasonic bath with isopropanol, dried, and weighed. The samples were weighted three times by a digital balance with an accuracy of 0.1 mg in order to determine the average value of mass loss. The eroded surface was tested by dye penetrant to reveal eventual crack propagation after erosion test. The erosion-test parameters and abrasive particles characteristics are given in Table 2.

4 Results and discussion

4.1 Effect of linear laser energy on erosion rate

During a typical laser cladding process, different process parameters would alter the thermal gradient, cooling cycle, and consequently the coating microstructure [19]. The effect of linear laser energy on the microstructural characteristics of the coatings was investigated by SEM-EDX analysis. As can be seen in Fig. 3, the WC grains stand out in the nickel-based alloy matrix. Partial dissolution of WC particles occurred during the laser cladding, which mainly consisted of eutectic carbides and primary carbides. EDX analysis revealed that both carbide phases consisted of (W, Cr, and Ni)$_x$C$_y$. The microstructure of Ni-binder featured dendrites and interdendrites. The dendrites shape of the coating fabricated by 315 J/mm of linear laser energy was mainly equiaxed indicating a presence of high cooling rate with this level of laser energy. This is a typical rapidly solidified microstructure during laser cladding in which the small volume of the molten pool cooled down through a sink of large substrate. EDX data showed that the Ni-based matrix was enriched with W (up to 5 %) that was mainly caused by partial dissolution of WC particles. In the coating with higher linear laser energy due to lower cooling rate, the eutectic grains were bigger in addition; the volume

Table 2 Slurry erosion test conditions and abrasive particle characteristics

Slurry erosion test conditions	Unit	Value
Stand-off distance	mm	1127
Mixing tube diameter	mm	1.2
Impinging angle	α^0	30,45,60,90
Exposure time	s	30–210
Water pressure	MPa	340
Abrasive flow rate	g/s	6.8
Hardness of garnet	Mohs	8/9
Abrasive particle size	µm	80–100
Particle approach velocity	m/s	56

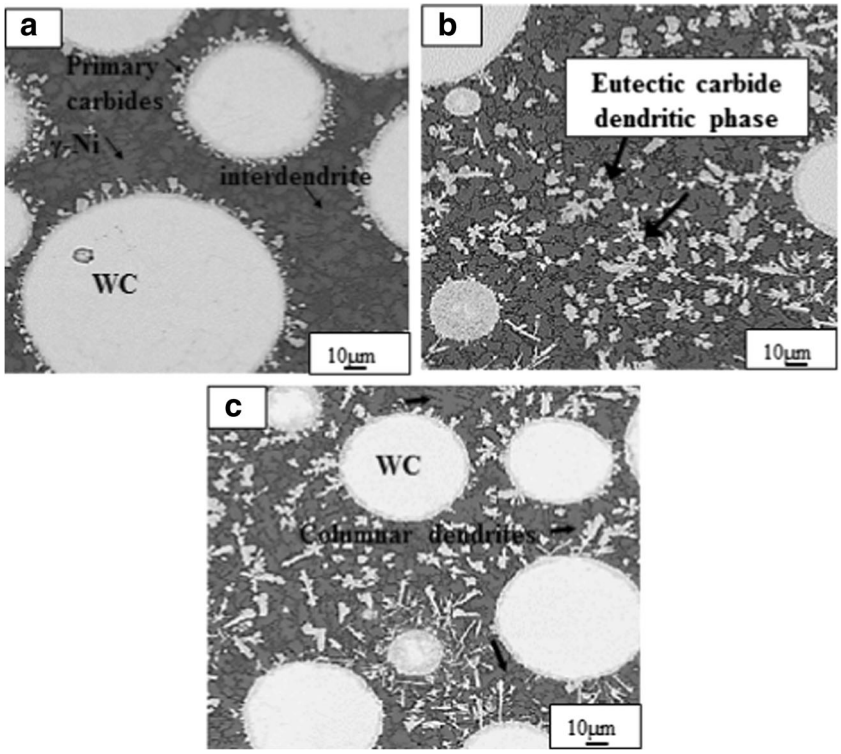

Fig. 3 Microstructure of the coating **a** with 315 J/mm linear energy, **b** 400 J/mm linear energy, and **c** 700 J/mm linear energy

fraction of dendrites was higher than interdendrites resulting in the grain coarsening.

In the coating with 700 J/mm of the linear laser energy, the presence of columnar shape of dendrites was limbed to the lower cooling rate at this level of linear laser energy (see Fig. 3c). The dendrite arms of the columnar structure growth outward of WC particle were limbed to the superior thermal properties of WC that acted as a heat sink in the Ni-matrix. The number of dissolved primary and eutectic carbides increased by increasing the linear laser energy (see Fig. 3c). This could be mainly attributed to the fact that WC is very prone to dissolution in the molten pool if sufficient time and temperature are provided. The dissolved WC particles could re-precipitate and formed secondary carbides (see Fig. 3b and c).

The coating microhardness is one of the most important mechanical properties in judging the erosion resistance of a coating, Fig. 4 compares the microhardness of the laser clads fabricated at three different laser energy densities. The hardness pattern clearly shows the decrease in hardness with the increase in laser energy density. The highest hardness of Ni-60 %WC coating is at 315 J/mm, followed by 400, and 700 J/mm. The hardness of Ni-60 %WC coating is generally attributed to the grain size of Ni binder, carbide phases, and the formed intermetallic phases during the cladding process. It has been shown [20] that there is an inverse linear relation between surface hardness and erosion rate.

The effect of linear laser energy on erosion resistance of fabricated coating was studied by using a dimensionless parameter (Fig. 5); namely, erosion value (EV):

$$EV = \frac{\Delta w}{F \times t} \tag{2}$$

$$R = \frac{1}{EV} \tag{3}$$

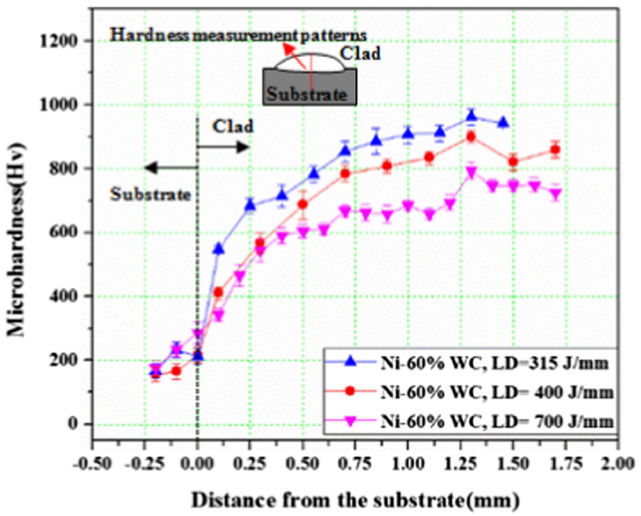

Fig. 4 Microhardness pattern of Ni-WC clad obtained under different linear laser energies

where F is feed rate of slurry jet (g/s), t is incremental exposure time (s), Δw is weight loss (g) per measuring increment, and R is erosion resistance. Figure 5 compares the erosion value of the laser cladded coupons for the exposure time up to 210 s at 90° impact angle. The coatings with higher laser energy density have higher erosion value that could be related to the lower hardness of coating. The increase in laser energy density from 315 to 700 J/mm decreased the erosion value by 40 %. The conclusion could be drawn that a defect free MMC coating fabricated by lower laser energy has finer microstructure and higher microhardness and consequently higher erosion resistance.

The erosion mechanism in Ni-WC MMC coating could be characterized as follow: the erosion model of a ductile material such as Ni-binder is in the form of ploughing scars and plastic deformation and for carbides the erosion model is in the form of the brittle fracturing and cracking. Conical, radial, and lateral cracks are formed in the region of impact with locale reduction of the strength of coating. When abrasive particles strike brittle material, cracks begin to propagate from the corner of the carbide particles due to the high concentrations of stress near the edge of the carbide particles. The cracks initiate and propagate when the particle impact force exceeds the threshold value of brittle material hardness and fracture toughness [21].

Depending on the properties of coated material, scars appearing at the impacted surface were found to vary in shape and size. Figure 6 shows a SEM micrograph of eroded coating surface with 315 and 700 J/mm linear laser energy at 90° impinging angle. The back scattering image of eroded surface showed the higher number of precipitated secondary carbides in the coating with 700 J/mm. Comparing the eroded surfaces of the coatings obtained under the different linear laser energies showed that the degree of the material removed and the depth of erosion footprint by abrasive particles were less in the coatings obtained under lower linear laser energy. This could be attributed to the higher hardness of the coating binder, higher resistance to material removal, and lower volume fraction of precipitated carbides. The higher magnification of eroded surface (see Fig. 6c) shows the microcutting and microploughing on the γ-Ni phase, where the consecutive impacts of the slurry jet promoted the formation and removal of the coated material. In this area, some of eroded debris has been adhered to the surface. The EDS analysis showed that the debris were typically located in the Ni-phase because Ni was softer phase.

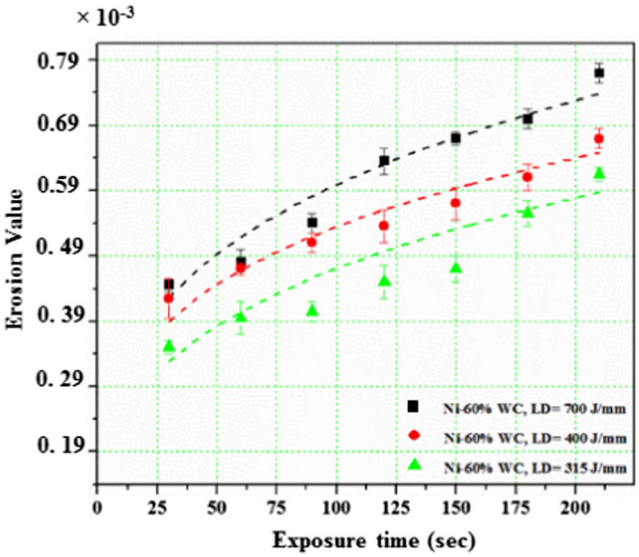

Fig. 5 Erosion value of Ni-WC coating at different laser energy densities

Higher degree of WC dissolution in the coating with higher linear laser energy would result in higher amount of secondary precipitated carbides and brittle intermetallic phases (see Fig. 6b). Therefore, as it is shown in Fig. 6d, the material would suffer from the brittle erosion mechanism. The erosion scars of the coating obtained under 700 J/mm of linear laser energy at 90° impact angle could be characterized as a severe surface damage including pits, cleavages, craters, and large cavities caused by WC pullouts. The pits and cleavages formation indicate that the erosion was mainly a consequence of surface fracture. At this angle of incident, the total kinetic impact energy was high enough to dramatically degrade the coated surface.

Generally, when high-velocity erosive particles struck the surface, the WC particles fractured. The Ni binder of the coating obtained under 700 J/mm of linear laser energy experienced heavy mass loss. The WC particles could easily be pulled out creating the deep micro-craters at the surface. These micro-craters made the surface more vulnerable to the erosion and directly affected the surface roughness. As a conclusion, the dominant erosion mechanism for the coating with higher linear laser energy was fracturing which is a characteristic erosion mechanism of brittle materials.

4.2 Effect of impact angle on erosion rate

Slurry erosion of composite materials depends on many factors including the mechanical properties of the target as well as the impact parameters such as an impact angle. The angle of impact along the other testing conditions determines the mechanisms and the rate of material damage and removal. The effect of the impact angle on the erosion value of Ni-60 %WC coatings obtained under different laser energy densities is shown in Fig. 7a. It is shown that the erosion value increased at higher impact angles. For all coating conditions, the maximum erosion rate occurred under a 90° impact angle. Several phenomena were responsible for the highest erosion value at a highest impact angle. An oblique impact angle resulted in a larger contact area and a lower impact force between the erodent particles and the coated surface. Additionally, at a lower impact angle, the particles tended to slide on

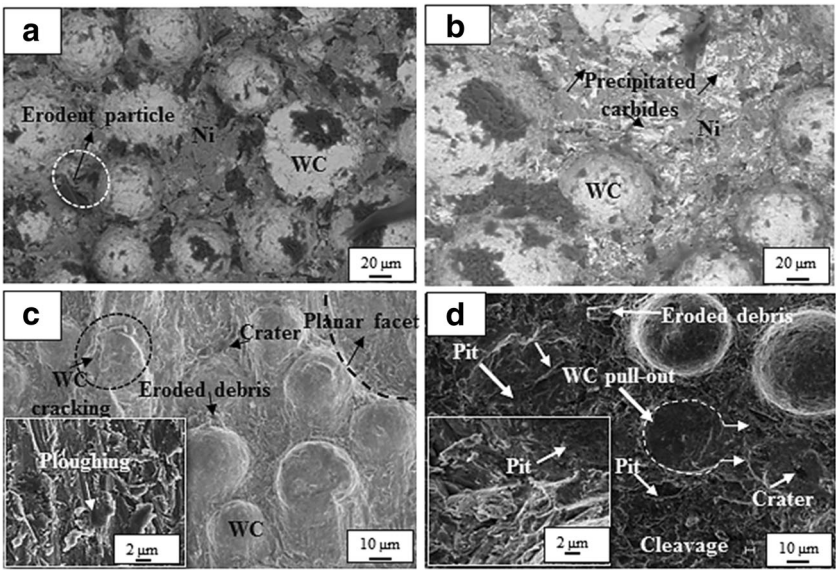

Fig. 6 SEM micrographs of surfaces after erosion test of Ni-60 %WC coatings at 90° **a** BSE image of eroded surface coating with 315 J/mm, **b** BSE image of eroded surface coating with 700 J/mm, **c** SE image eroded surface coating with 315 J/mm, **d** SE image eroded surface coating with 700 J/mm

the surface rather than impact the surface causing an abrasion-driven erosion pattern. At high impact angle (90°), the transferred impact energy from the erodent particles to the eroded surface is higher. The majority part of impact kinetic energy would be transformed to the target surface causing the material removal.

Furthermore, the results showed that the deviation of the erosion rate between coatings fabricated with different laser energy densities at the lower impact angle (30°) was small, at low impact angle the behavior of Ni-WC coating is close to ductile material and main mechanism for material removal is ploughing and plastic deformation of Ni-binder. At a 90° impact angle, the effect of the laser energy density was more apparent, because the level of induced stress is higher, erosion mechanisms is based on crack propagation from the carbide particles, and the main coating behavior under erosion is close to brittle material. In such this condition, the harder coating (lower laser energy density) absorbed less kinetic energy of impinging particles; therefore, the erosion value was lower. Figure 7b–d compare the erosion scar profiles of the coatings obtained with 400 J/mm at 30 and 90° impact angles. The characterization of eroded surface could be done by the degree of energy absorption in the erosion test and the dominant erosion profiles. During erosion when the particles impact the surface, assuming that the erodent particles were not deformed, their kinetic energy would be transferred to the target

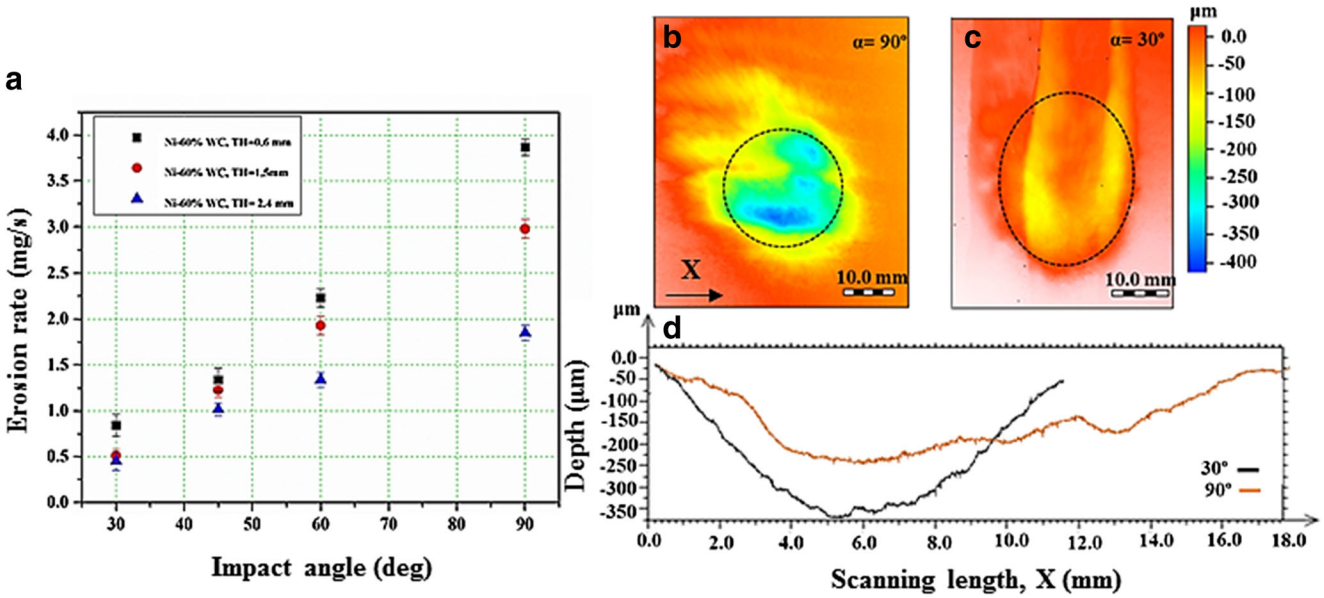

Fig. 7 **a** The effect of impact angle on the erosion rate of the coatings of different thicknesses, **b** and **c** 2D depth profiles of the Ni-60 %WC coatings captured by optical profilometer: for a 90° impact angle and a 30° impact angle, respectively, **d** comparison of profiles of erosion scars at different impact angles

through elastic and plastic deformations. Most of the elastic energy would be released while the plastic energy would plastically deform the target material. Therefore, the size of the eroded surface could be used to represent the input energy. The qualitative observation of the eroded surface at different impact angles was characterized by an optical profilometer with a 1-μm scanning step. Figure 7c shows the samples tested under a 30° impact angle, which have a longer, nearly elliptical contact areas and shallower erosion scars. The depth of erosion profile varied from 210±3 μm for 30° to 330 ±3 μm for 90°, while the size of the eroded surface was 400 and 280 mm^2 for the 30 and 90° orientations, respectively. The scar volume for the 30° impact angle was 84 and 92.4 mm^3 for the 90° impact angle.

The impact angle also affected the eroded surface roughness, due to the governing impact mechanisms at different angles. Figure 8 presents the effect of impact angle on the surface roughness of Ni-60 %WC for the coating with 400 J/mm linear laser energy. The maximum roughness, Ra occurred at the 90° impact angle with a value of 17.2 μm while the minimum roughness was 7.8 μm that occurred at 30° impact angle. The scanned surface for each impact angle showed the degree of the surface roughness. The optical profile of the eroded surface showed a smooth surface without any deep craters for the impact angle of 30°. The roughness of the optical profile at 90° of the impact angle indicated that the impinging slurry jet hit the surface with the high energy leaving a crater footprint. Therefore, the possibilities for crack initiation, micro-pit generation, cavity formation, and granular fracture were increased at 90° of impact angle.

4.3 Effect of adding nano-WC particles on erosion rate

It has been shown [18] that the microstructural properties of the coating and size of the carbides particles are the prevalent surface coating characteristics that affect the erosion rate of the coating. A coating material with finer microstructure can withstand induced strain by impinging particles for longer period of time [22]. Additionally, the nanocrystalline grain structure has the potential to dramatically improve the mechanical properties of the hard-facing material [23]. Previous studies show [24] that the particle size of the carbides in hard-facing materials has also a substantial effect on the erosion rate of these materials. Variation of carbide size and its distribution would affect the erosion behavior of the coating. The addition of nano scale WC particles to the Ni-WC coating enhances the strength of the coating by dispersion the nanoparticles between micro carbides and reinforcing the Ni-binder. Yarrapareddy and Kovacevic [9] showed that the nano-based coating exhibits better performance under the erosion by strengthening the matrix. They showed by adding 5 % nano-WC to Ni-WC coating, the penetration depth after erosion under 45° impact angle decreased from 0.85 to 0.7 mm. Balu et al. [25] also show that addition of 10 % nano-WC particles enhance the microhardness around 12 % of the coating and subsequently increase the coating erosion resistance up to 36 % at 60° impact angle.

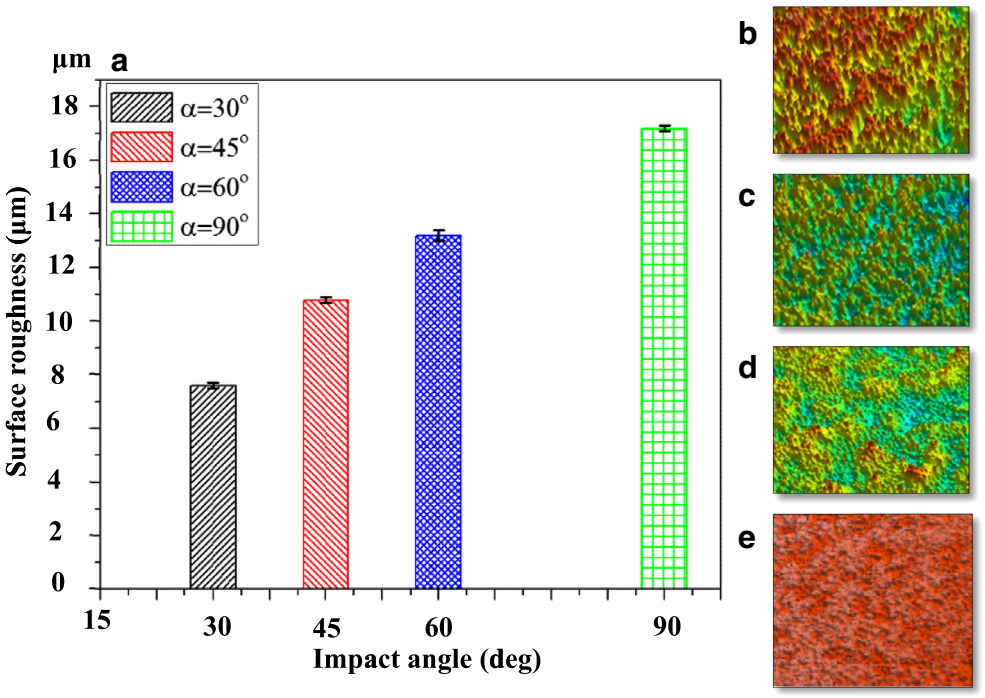

Fig. 8 **a** The surface roughness of the Ni-60 %WC coatings at different impact angles, captured eroded surface by profilometer **b** at 90°, **c** at 60°, **d** at 45 °, **e** at 30°

The microstructure of coating with addition of 5 % nano-WC is shown in Fig. 9. The addition of nano-WC into the coating increased the ratio of surface area of the carbides per unit volume. This led to a finer microstructure of the binder and more uniform WC distribution. Figure 9b shows the overall microstructure of the coating with nano-WC consists of the γ-Ni dendrites phases (marked 1) and some small blocky carbides (marked 2) in the Ni-matrix that was a combination of agglomerated nano-WC particles and precipitates WC in an Ni-alloy solvent. The nano-WC particles had a preferential melting due to the higher energy of contact points between closely spaced nanoparticles, causing the formation of large clusters (marked 2 in Fig. 9b). The uniform distribution of blocky carbides along the clad enhanced the hardness of the coating. Comparing the microstructure of Ni-binder (see Fig. 9c, d) shows the average grain size of the Ni-matrix with adding nano-WC particles is finder (1 μm) than in the Ni-60 %WC coating of (3 μm). The addition of nano-WC to the Ni-WC coating could improve the microhardness and fracture toughness of the coating [23, 26, 27]. In this study, the effect of adding nano-WC particles was investigated by adding nanoparticles as three different mass fractions: 3, 5, and 10 wt%, respectively. The effect of added nano-WC on the erosion resistance was investigated by measuring the erosion value under different impact angles.

Figure 10a shows the erosion value as a function of the impact angle of the coatings modified with nano-WC compared as well as for a non-modified Ni-WC coating, for a 210-s exposure time. At all impact angles, the mass loss of the coatings with added nano-WC decreased. The minimum mass loss among the examined coatings was a coating modified with 5 % nano-WC. In the coatings modified by nano-WC, a contributing factor to the lower erosion value was the higher hardness of the binder. The larger WC grains were more readily cracked and chipped off than in the case of smaller WC particles.

Additionally, the introduction of nano-WC to the coating increased the ratio of the surface area of the carbides with respect to Ni-matrix per unit volume. This increase led to a finer microstructure of the binder and more uniform WC distribution. Fang et al. [23] reported that the fracture toughness of the MMC coatings by adding nanoparticles improved because of the reduction in the grain size and number of microscopic flaws. Additionally, as the grain size was reduced, the area of interfaces between WC and Ni-matrix increased. Therefore, the grain interfaces opposed the crack path and its propagation [23]. Figure 10b compares the volume loss of Ni-WC coating with nano-WC versus the coating hardness at the impact angle of 90°. There was an approximately inverse log-linear relationship between the target hardness and volume loss. It is shown that the volume loss decreased for the coatings modified with nano-WC. A 5 % nano-WC showed the best performance where the mass loss was reduced for 30 % comparing to unmodified Ni-60 %WC cladding. This figure also shows that addition of nano-WC increases the microhardness to the level of 1400 HV_{500g}. The increase in the microhardness by adding nano-WC particles could be attributed to the enhancement of the WC distribution and decrease the mean free path (area of Ni binder between the two adjacent WC particles). It should be mentioned that no significant improvement in the coating microhardness and erosion value was observed by adding 10 % nano-WC. This could be attributed to a high density of aggregation of nano-WC particles causing the porosity and non-uniform distribution of nanoparticles. Based on the results shown in Fig. 10, it could be concluded that the optimum mass fraction of nano-WC particles

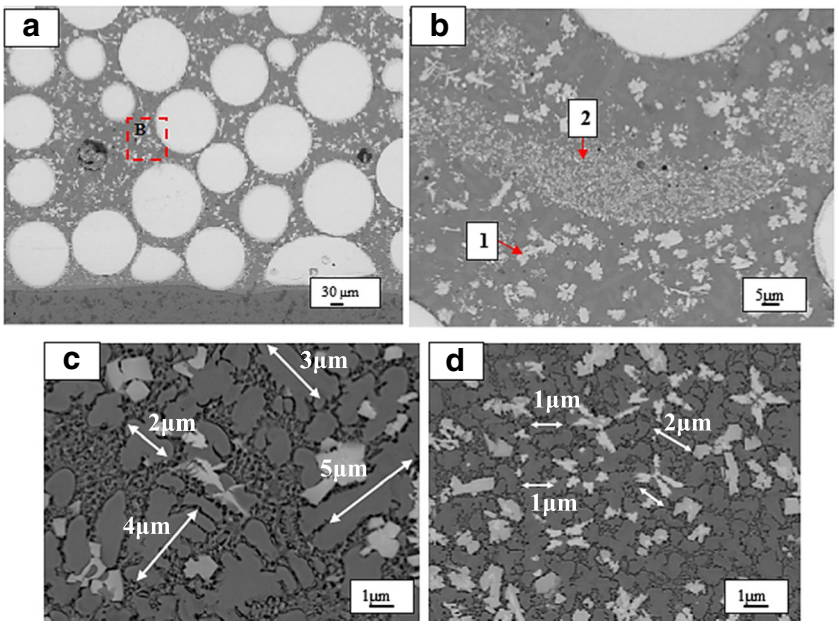

Fig. 9 **a** Overall view of coating modified with 5 % nano-WC, **b** higher magnification of B area microstructural features, **c** microstructure of Ni binder in Ni-60 %WC coating, **d** microstructure of Ni-binder of Ni-55 % WC–5 % nano-WC coating

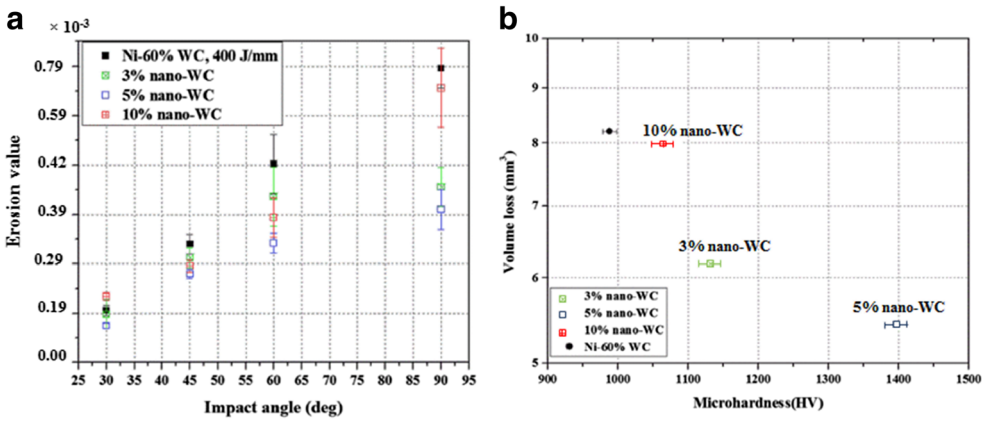

Fig. 10 **a** Erosion value of Ni-WC coating versus impact angle for different mass fractions of nano-WC, **b** volume loss versus coating hardness for different mass fractions of nano-WC

with respect to the improvement in the microhardness and erosion resistnace should be at 5 wt%.

The SEM micrographs of worn surfaces of Ni-WC coating with addition of 5 and 10 wt% of nano-WC particles under 90° of impact angle are shown in Fig. 11. The back scattering images of eroded surfaces (see Fig. 11a, b) showed the uniform distribution of secondary carbides among the primary WC particles. In coating with 10 % nano-WC, the combination of aggregated nano-WC particles and secondary carbides, forming a large cluster, could be observed. The number of craters, pits, and cleavages in the Ni-WC coating with added nano-WC particles decreased in comparison to the worn surface of Ni-60 %WC coating, demonstrating the increase in the erosion resistance. Furthermore, WC pullout was not observed, indicating a strong bonding between the WC particles and the Ni-binder. The impact of high velocity abrasive particles at a 90° impingement angle caused the fracture and corner chipping off WC grains (Fig. 11c). The shallow grooves and scratches manifest the low degree of erosion of the coating with 5 % nano-WC. The lack of pit and deep cavities in the worn surface with 5 % nano-WC clearly demonstrated the effect of higher hardness of this coating on the erosion resistance as a result of the reinforcement of the Ni-binder by nano-WC particles and secondary carbides. The traces of the deep and abundant cleavages in metallic phase in the eroded surface of the coating with 10 % nano-WC indicate the higher erosion value and material loss in comparison to the coating with 5 % nano-WC.

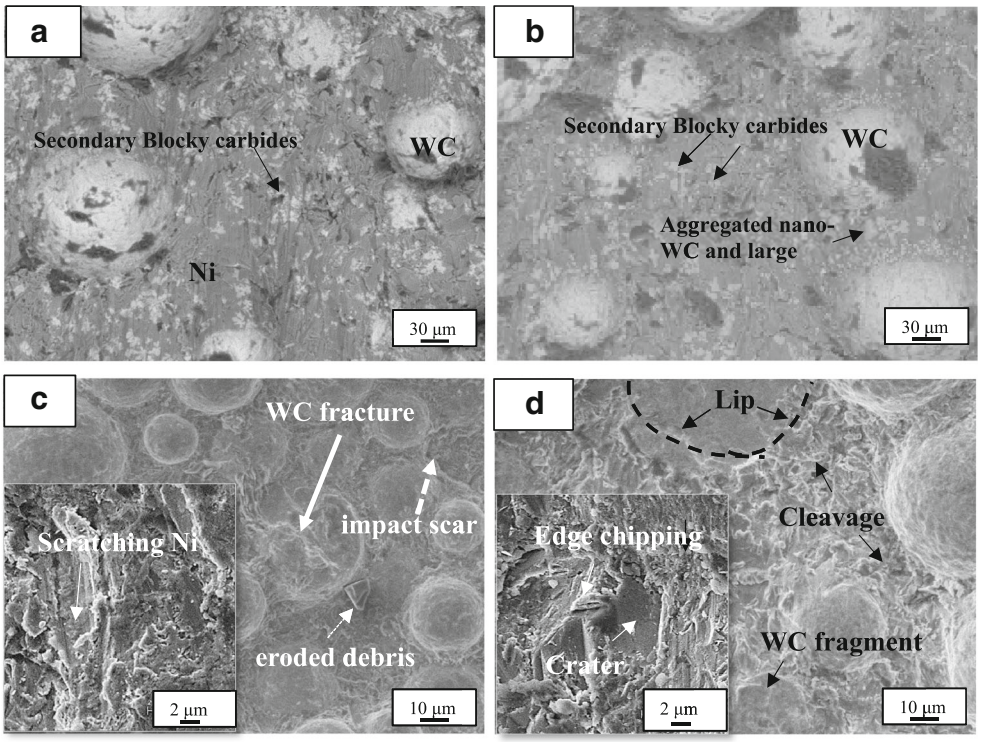

Fig. 11 SEM micrographs of worn surfaces after erosion testing of Ni-WC coatings at 90° **a** BSE image of eroded surface coating with 5 % nano-WC, **b** BSE image of eroded surface coating with 10 % nano-WC, **c** SE image of eroded surface coating with 5 % nano-WC, **d** SE image of eroded surface coating with 10 % nano-WC

4.4 Effect of adding rare earth (RE) element (La_2O_3) particles on erosion rate

In recent years, the RE elements were gradually introduced to the laser surface treatment area [21, 28]. The addition of the RE elements is believed to have beneficial effects on resistivity of the coatings exposed to erosive and corrosive environments [11]. Due to the particular atomic structure and outstanding chemical appetence, RE elements possess excellent physical and chemical characteristics [21]. Furthermore, the RE elements purify microstructure (i.e., chemical reaction by specific elements that forms slag) and eliminate pores and micro-cracks.

In this study, the effect of using La_2O_3 as an RE element in three different mass fractions (0.5, 1.0, and 2.0 %) on microstructural properties, chemical composition, microhardness of the coating, and subsequently, the erosion resistance of the coating was investigated. The cross-section micrographs of the coatings with La_2O_3 addition show that homogenous coating with the even distribution of the big and small WC particulates in the surrounding matrix was achieved by adding 1 % of La_2O_3. The microstructure of the coating with 1 % La_2O_3 is shown in Fig. 12. Two different shapes of secondary carbides were observed in the coating with addition of La_2O_3: bar-like or lamellar carbides (marked by 1 in Fig. 12b) and butterfly carbides (marked by 2 in Fig. 12b). The La_2O_3 could increase the latent heat of melting, reduce liquid temperature, and increase the solid temperature that could result in a decreased grain size as well as in the formation of the precipitated carbides as lamellar carbides [11, 28]. Furthermore, La_2O_3 could prevent the accumulation of the lamellar secondary carbides near the vicinity of the primary carbides [21]. Therefore, stress concentration around the primary carbides could decrease. However, if the number of lamellar carbides exceeded a specific range, the crack possibility could increase [17]. This increase might be attributed to the needle-like shape of the lamellar carbides that could turn these carbides into the stress concentration sites instead of the hard-phase particles. The large fraction of secondary phases formed in the coating modified by La_2O_3 could be the consequence of the high concentration of alloying elements and the dissolution of certain amount of WC manifesting in the increase in the hardness of coating [11]. It is clear in Fig. 12c and d that the number of precipitated carbides comparing with unmodified Ni-60 %WC was increased. This could mainly attribute to changing the solidification regime in coating modified by La_2O_3 as described before.

The effect of addition of La_2O_3 on chemical composition of Ni-WC coating was studied by an XRD analysis. Figure 13 compares the possible chemical phases in coating with and without La_2O_3 modification of Ni-WC coating based on XRD analysis. The overall phase identification has shown that the major phases in coatings were γ-Ni with a cubic crystal structure and WC, W_2C, and CW_3 with a hexagonal crystal structure. The addition of La_2O_3, as the surface active element that reacts easily with oxygen, carbon, and some stable compounds caused the formation of new phases such as La_2NiO_2, LaC_2, and $La_2Ni_5C_3$. In addition, some peaks corresponding to WO_3 were found. The Cr_7C_3, an intermetallic phase with high hardness, was also observed in the modified coating by La_2O_3. In coating with La_2O_3, a portion of the composed phases was gathered at the top of the molten pool and after

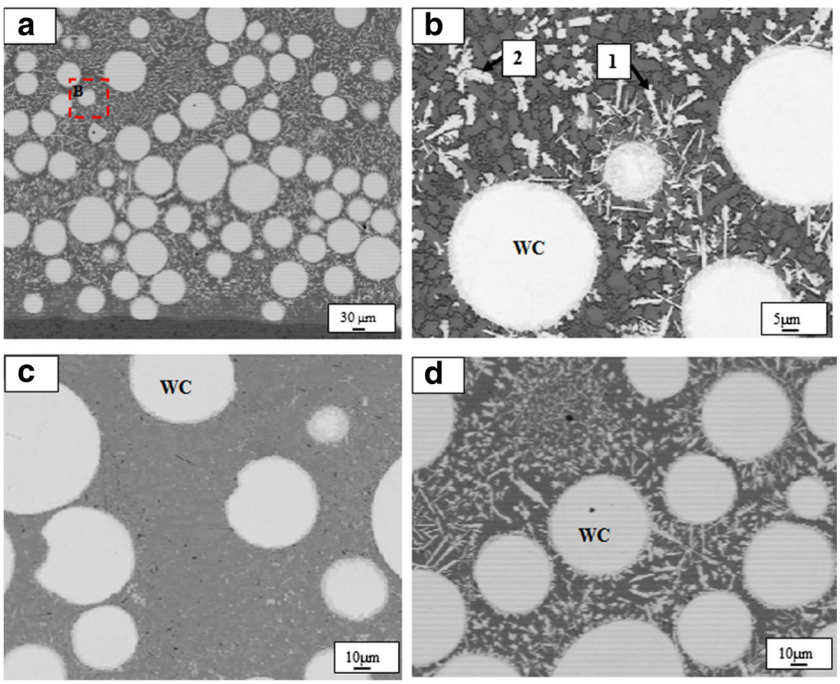

Fig. 12 **a** Overall view of coating modified by 1 % of La_2O_3, **b** higher magnification of microstructural features in B area, **c** SE image of unmodified Ni-60 %WC coating, **d** SE image of Ni-WC modified with 1 % La_2O_3

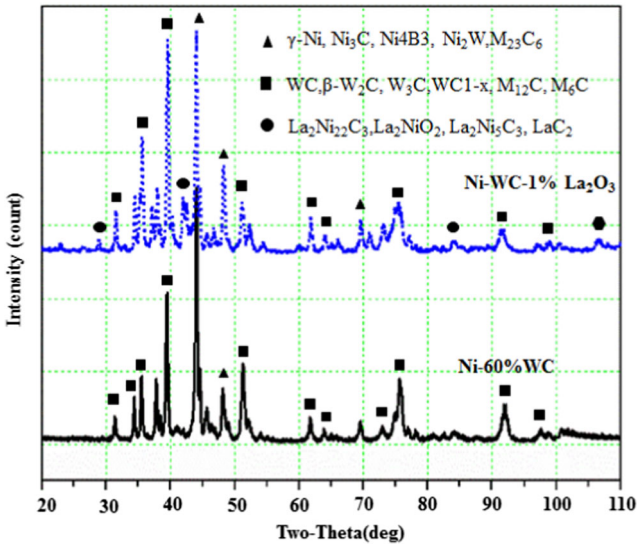

Fig. 13 XRD spectra for Ni-60 %WC and Ni-WC-1 % La_2O_3 coating

the solidification a slag (purification) was formed, while a portion of it stayed in the clad forming composed phases. Thus, by alloying the Ni/WC composite coating with RE element, the inclusion content within the coating would be decreased and the coating would be more purified by deoxidation [28].

The effect of adding the RE element (La_2O_3) on the erosion resistance of the coating was studied according to the erosion value and volume loss under different impact angles. Figure 14 compares the erosion value and volume loss of the Ni/WC coatings with and without La_2O_3 after 210-s exposure time. It is shown that the maximum improvement of erosion value was achieved for a coating with 1 % La_2O_3, under impact angle of 90°. In the coating modified with La_2O_3, the minimum erosion improvement belongs to the coating modified with 2 % La_2O_3 due to the inhomogeneous WC distribution in this coating (see Fig. 1h). Therefore, according to erosion value of coating modified with La_2O_3, the optimal mass fraction of La_2O_3 is 1 %. The coating modified with 1 % mass fraction of La_2O_3 had a uniform distribution of carbides particles and lowest erosion value.

Figure 14b compares the volume loss versus the coating microhardness for different mass fraction of La_2O_3 at 45° impact angle. It is shown that the microhardness of the coating with La_2O_3 addition increased, this could be attributed to the grain-refinement effect and formation of new intermetallic compounds. The addition of La_2O_3 has promoted the formation of $La_2Ni_{22}C_3$ and some intermetallic phases such as Cr_7C_3. According to the results shown in Fig. 14, it could be concluded that the optimum mass fraction of La_2O_3 with respect to the erosion resistance of the coating should not be larger than 1 %.

The SEM micrographs of worn surfaces of Ni-WC coating with 1 and 2 wt% of La_2O_3 under 90° impact angle are shown in Fig. 15. The back scattering images of eroded surfaces treated by La_2O_3 (see Fig. 15a, b) show the higher volume fraction of lamellar and butterfly shapes of secondary carbides than in the case of unmodified Ni-60 %WC coating (see Fig. 6a, b). The morphology of eroded surfaces presents the dominant brittle erosion behavior in the coatings modified by La_2O_3 due to high volume fraction of secondary carbides. The brittle behavior of lamellar carbides would result into cracking and edge chipping and consequently cleaving. The cleavages were formed as a result of the cracks intersections and delamination. The cleavages in the coating modified by La_2O_3 were confined into a small area. The key role of La_2O_3 during the cladding is in making the microstructure grains finer and consequently more grain boundaries could restrain the crack

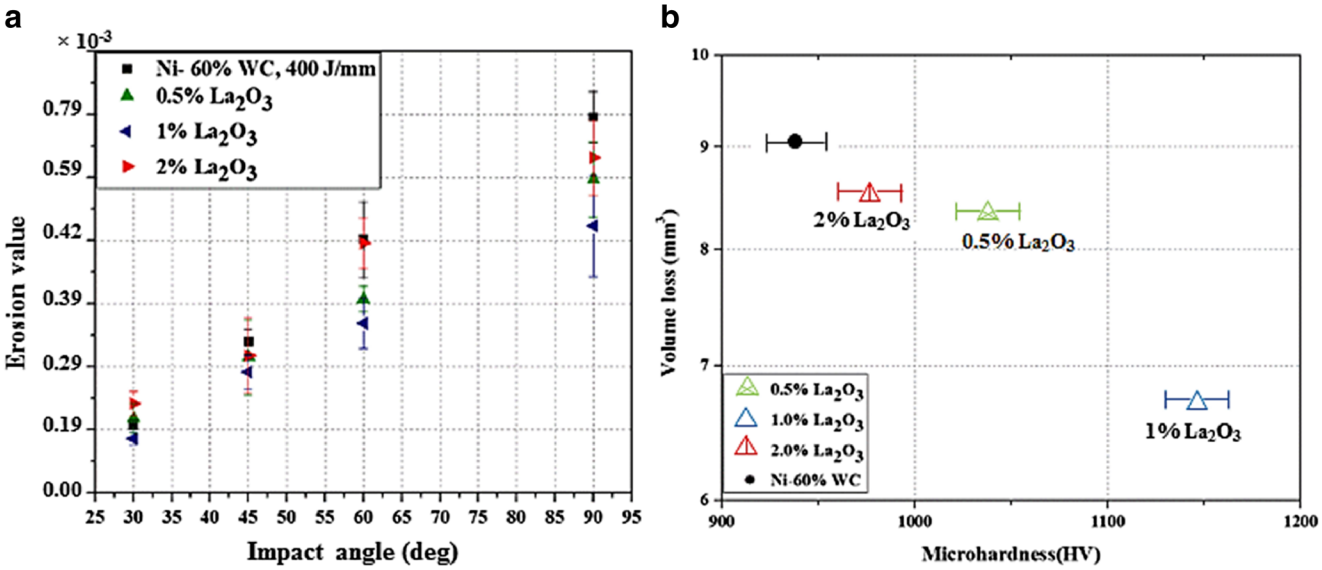

Fig. 14 **a** Erosion value of Ni-WC coating versus impact angle for different mass fractions of La_2O_3, **b** volume loss versus coating hardness for different mass fraction of La_2O_3

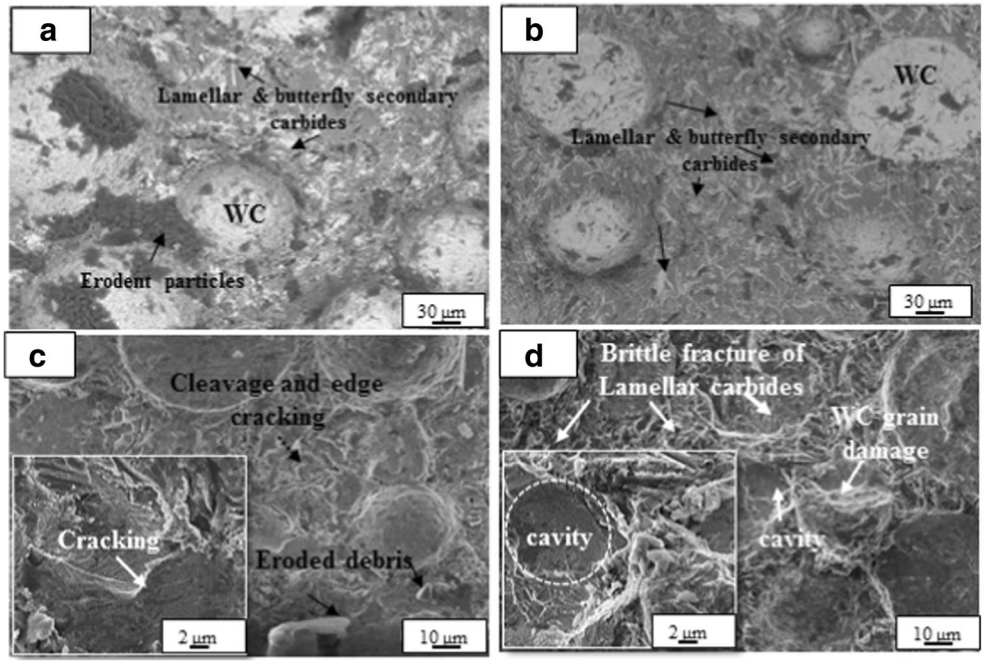

Fig. 15 SEM micrographs of worn surfaces after erosion testing of Ni-WC coatings at 90° of impact angle **a** BSE image of eroded surface coating by 1 % of La_2O_3, **b** BSE image of eroded surface coating by 2 % of La_2O_3, **c** SE image eroded surface coating by 1 % of La_2O_3, **d** SE image eroded surface coating by 2 % of La_2O_3

propagation and prevent the degradation of a large area. The number of deep scratches and grooves in coating with 1 % of La_2O_3 in comparison to Ni-60 %WC eroded surface (see Fig. 6c) decreased because of the reinforcement of the Ni-matrix by secondary carbides. However, immense presence of secondary carbides in the coating with 2 % of La_2O_3 increased the stress concentration under erosion and caused deep cavities and higher mass loss. According to the erosion responses (i.e., erosion value and volume loss) of the coatings modified with three mass fractions of nano-WC and La_2O_3, it was found that the optimum mass fraction for nano-WC was 5 % and for La_2O_3 was 1 %. The optimum mass fraction occurred at the point that corresponds to the highest hardness and the lowest erosion rate. It is also worth to compare the coating erosion resistivity at the optimum mass fractions of nano-WC (5 %) and La_2O_3 (1 %).

Figure 16 compares the erosion values between coatings with optimum mass fractions. For all impact angles, the coatings with 5 % of nano-WC had the least erosion value. The erosion values of the coatings modified by nano-WC were comparatively lower than the erosion values for coatings modified by La_2O_3; such difference could be attributed to the shape of the secondary carbides in the coatings and corresponding hardness. The dominant secondary carbide shape in coating could play an important role in erosion resistivity. The secondary carbide shape in the coating with nano-WC was of mainly blocky carbide shape, while the coating with La_2O_3 had lamellar and butterfly shapes. The cracks easily would nucleated and propagated from the lamellar carbides because of its geometry (i.e., stress concentration due to needle-like shape). Additionally, the chemical phases formed in the reaction with La_2O_3 could have contributed to the decrease in hardness [29].

The erosion scars and surface roughness of the Ni-WC coatings with an optimum mass fraction of nano-WC and La_2O_3 at the impact angle of 45° are shown in Fig. 17. The material losses from the coatings, going form the largest to the smallest one, were in order as: Ni-60 %WC, Ni-WC-1 %

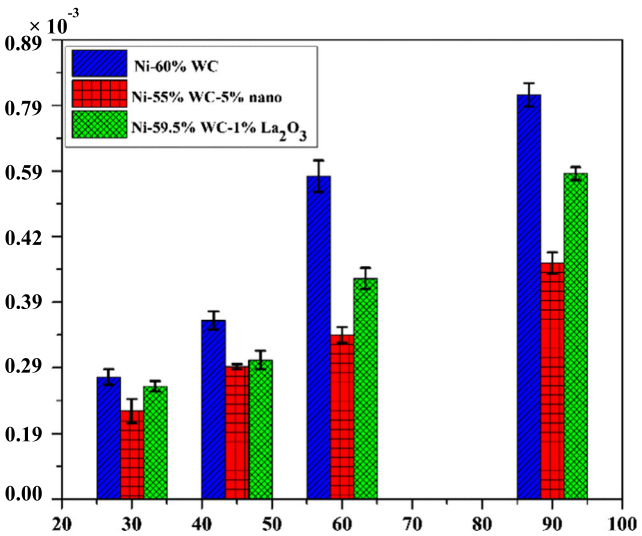

Fig. 16 **a** Effect of different mass fractions of nano-WC and La_2O_3 on the coating hardness and its erosion rate, **b** comparing the mass loss of the coatings with optimum mass fraction of nano-WC and La_2O_3 and conventional Ni-60 %WC

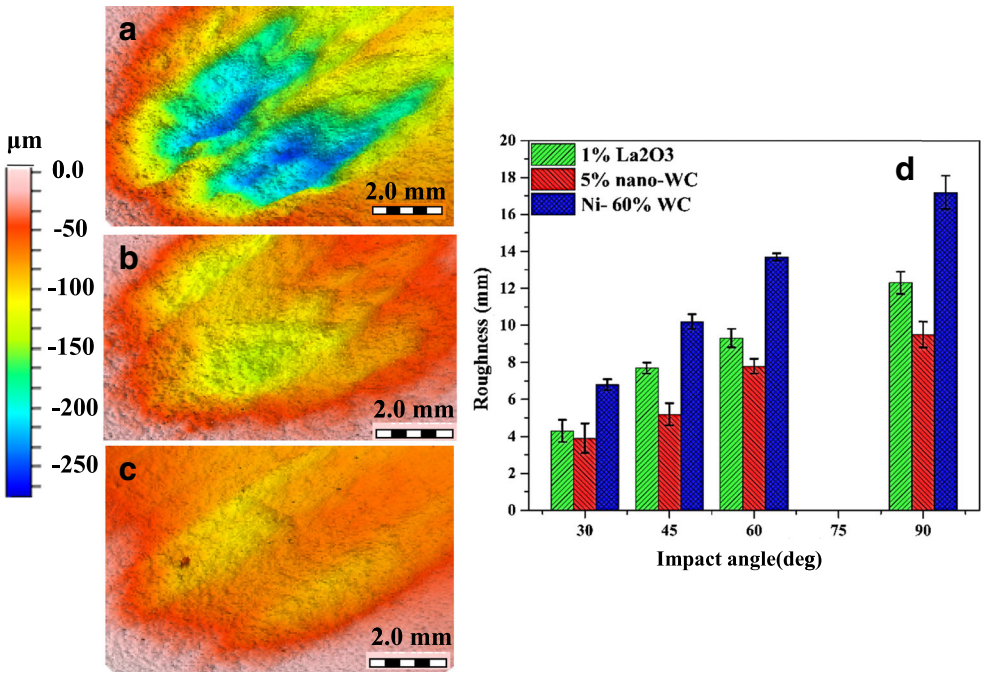

Fig. 17 3D profiles of the eroded surfaces of **a** Ni-60 %WC, **b** Ni-WC-1 % La2O3, **c** Ni-WC-5 % nano-WC, **d** comparison between roughness of the coatings at different impact angles

La_2O_3, and Ni-WC-5 % nano-WC, respectively. Figure 17d compares the eroded surface roughness of the different coatings at three impinging angles (30, 45, 60, and 90°). All coating compositions showed a maximum eroded surface roughness at a 90° of impact angle as the consequence of high impact energy and surface degradations caused by a cutting action, chip formation, and pullout of the WC particles. Coatings with higher hardness showed a lower roughness. Additionally, there were no deep cavities or pits formed by plastic deformation. Coatings with lower hardness resulted in a higher surface roughness, because of the pitting due to chip creation, pullout of the WC grains from the weak matrix, and the subsequent formation of deep cavities.

5 Conclusions

The erosion behavior of laser-cladded Ni/WC coatings under different laser energy densities and modified with nano-WC particles and La_2O_3 was studied. The slurry erosion tests were executed at an AWJ machine at the different impact angles. Based on the results of this study, the following conclusions could be drawn:

- A dimensionless erosion value was introduced to quantify the erosion resistance of Ni-WC MMC coatings. The erosion value of laser cladded coatings showed a linear relationship with the exposure time.
- The laser energy density in fabricating the laser cladded coatings had a great influence on the slurry erosion resistance. The Ni-60 %WC fabricated with 315 J/mm^2 showed higher erosion resistance than coatings fabricated with 400 and 700 J/mm^2.
- The Ni-WC composite coating showed a tendency for an inverse log-linear relationship between coating hardness and matrix volume loss.
- At low impact angles, the erodent particles slid on the surface and generated grooves on the soft Ni matrix because of the ductile material properties. Repeated impacts led to degradation of the matrix phase. Meanwhile, the reinforcing phase was subjected to brittle fracture, which led to the fracture propagation across the carbide grains.
- The addition of nano-WC strengthened the Ni-60 %WC coating by dispersing between micro-WC particles and decreasing the grain size of Ni matrix. The aggregation of nano-WC particles with dissolved WC forms the blocky secondary carbides that could enhance the erosion resistivity of the coating.
- The modification of coating with La_2O_3 powder increased the erosion resistance of the coating. The improved mechanical properties of La_2O_3 were a result of a purified coating and finer grain size with La_2O_3.
- The 5 % nano-WC coating showed the highest hardness value and lowest erosion rate. The 1 % La_2O_3 coating had an erosion rate higher than that of the conventional Ni-60 %WC coating but lower than the nano-WC coatings.
- The roughness of eroded surface at higher impact angle is higher due to the presence of deep cavities and cleavages. The coating modified with optimum mass fraction of nano-WC and La_2O_3 had relatively lower eroded surface roughness.

Compliance with ethical standards The authors had full access to all of the data in this study and take complete responsibility for the integrity of the data and the accuracy of the data analysis. This work was financially supported by NSF's Grant IIP-1034652. The authors acknowledge research engineer, Mr. Andrzej Socha at the Research Center for Advanced Manufacturing (RCAM) for his help in conducting the experiments and Roy Beavers in Geology department for his help in SEM, X-Ray, and EDS analyses at Southern Methodist University (SMU).

References

1. Nøkleberg L, Søntvedt T (1995) Erosion in choke valves—Oil and gas industry applications. Wear 186:401–412
2. Walley SM, Field JE, Greengrass M (1987) An impact and erosion study of polyether etherketone. Wear 114:59–71
3. Levin BF, Vecchio KS, DuPont JN, Marder AR (1999) Modeling solid-particle erosion of ductile alloys. Metall Mater Trans A30(7): 1763–1774
4. Upadhyaya GS (1998) Cemented tungsten carbides: production, properties and testing. William Andrew
5. Paul CP, Mishra SK, Tiwari P, Kukreja LM (2013) Solid-particle erosion behaviour of WC/Ni composite clad layers with different contents of WC particles. Opt Laser Technol 50:155–162
6. Gant AJ, Gee MG (2009) Structure–property relationships in liquid jet erosion of tungsten carbide hardmetals. Int J Refract Met Hard Mater 27(2):332–343
7. Meng H, Zhang Z, Zhao F, Qiu T (2013) Preparation of WC nanoparticles by twice ball milling. Int J Refract Met Hard Mater 41:191–197
8. Cho J, Joshi MS, Sun CT (2006) Effect of inclusion size on mechanical properties of polymeric composites with micro and nano particles. Compos Sci Technol 66(13):1941–1952
9. Yarrapareddy E, Kovacevic R (2008) Synthesis and characterization of laser-based direct metal deposited nano-particles reinforced surface coatings for industrial slurry erosion applications. Surf Coat Technol 202(10):1951–1965
10. Wang KL, Zhang QB, Sun ML, Wei XG, Zhu YM (2001) Rare earth elements modification of laser-clad nickel-based alloy coatings. Appl Surf Sci 174(3):191–200
11. Farahmand P, Liu S, Zhang Z, Kovacevic R (2014) Laser cladding assisted by induction heating of Ni–WC composite enhanced by nano-WC and La 2 O 3. Ceram Int 40(10):15421–15438
12. Parisa F, Balu P, Kong F, Kovacevic R (2013) Investigation of thermal cycle and hardness distribution in the laser cladding of AISI H13 tool steel produced by a high power direct diode laser. ASME 2013 International Mechanical Engineering Congress and Exposition. Am Soc Mech Eng
13. Mann BS, Vivek A, Pant BK (2013) High-power diode laser surface treated HVOF coating to combat high energy particle impact wear. J Mater Eng Perform 22(7):1995–2004
14. Farahmand P, Kovacevic R (2014) An experimental–numerical investigation of heat distribution and stress field in single-and multi-track laser cladding by a high-power direct diode laser. Opt Laser Technol 63:154–168
15. Zhou S, Huang Y, Zeng X, Qianwu H (2008) Microstructure characteristics of Ni-based WC composite coatings by laser induction hybrid rapid cladding. Mater Sci Eng A 480(1):564–572
16. Tian YS, Chen CZ, Chen LX, Huo QH (2006) Effect of RE oxides on the microstructure of the coatings fabricated on titanium alloys by laser alloying technique. Scr Mater 54(5):847–852
17. Zhao GM, Wang KL (2006) Effect of La2O3 on corrosion resistance of laser clad ferrite-based alloy coatings. Corros Sci 48(2):273–284
18. Kleis I, Kulu P (2008) Solid particle erosion. Occurrence, Prognosification and Control
19. Farahmand P, Kovacevic R (2014) Parametric study and multi-criteria optimization in laser cladding by a high power direct diode laser. Lasers Manuf Mater Proc 1(1–4):1–20
20. Wood RJK (2006) Erosion–corrosion interactions and their effect on marine and offshore materials. Wear 261(9):1012–1023
21. Gu D, Shen Y (2008) The role of La2O3 in direct laser sintering of submicrometre WC–Cop/Cu MMCs. J Phys D Appl Phys 41(9): 095308
22. Ball A (1983) On the importance of work hardening in the design of wear resistant material. Wear 91:201
23. Fang ZZ, Wang X, Taegong R, Hwang KS, Sohn HY (2009) Synthesis, sintering, and mechanical properties of nanocrystalline cemented tungsten carbide—a review. Int J Refract Met Hard Mater 27(2):288–299
24. Castberg TS, Johnsen R, Berget J (2013) Erosion of hardmetals: Dependence of WC grain size and distribution, and binder composition. Wear 300(1):1–7
25. Balu P, Hamid S, Kovacevic R (2013) An experimental study on slurry erosion resistance of single and multilayered deposits of Ni-WC produced by laser-based powder deposition process. J Mater Eng Perform 22(11):3398–3413
26. Liu S, Farahmand P, Kovacevic R (2014) Optical monitoring of high power direct diode laser cladding. Opt Laser Technol 64:363–376
27. Kosel TH (1992) Solid particle erosion. ASM Handb 18:199–213
28. Wang KL, Zhang QB, Sun ML, Wei XG (2003) Microstructural characteristics of laser clad coatings with rare earth metal elements. J Mater Process Technol 139(1):448–452
29. Haghi AK, Oluwatobi SO, Josmin PJ, Hanna JM, eds (2013) Composites and nanocomposites. CRC Press